Inorg. Chem. **2009**, *48*, 735−743

Synthesis and Characterization of Iron(II) Complexes with Tetradentate Diiminodiphosphine or Diaminodiphosphine Ligands as Precatalysts for the Hydrogenation of Acetophenone

Christine Sui-Seng, F. Nipa Haque, Alen Hadzovic, Anna-Maria Pütz, Valerie Reuss, Nils Meyer, Alan J. Lough, Marco Zimmer-De Iuliis, and Robert H. Morris*

Department of Chemistry, University of Toronto, 80 St. George St., Toronto, Ontario M5S 3H6, Canada

Received August 9, 2008

Six complexes of the type *trans*-[Fe(NCMe)$_2$(P−N−N−P)]X$_2$ (X = BF_4^-, B{Ar^f}$_4^-$) (Ar^f = 3,5-(CF$_3$)$_2$C$_6$H$_3$) containing diiminodiphosphine ligands and the complexes *trans*-[Fe(NCMe)$_2$(P−NH−NH−P)][BF$_4$]$_2$ with a diaminodiphosphine ligand were obtained by the reaction of Fe(II) salts with achiral and chiral P−N−N−P or P−NH−NH−P ligands, respectively, in acetonitrile at ambient temperature. The P−N−N−P ligands are derived from reaction of ortho-diphenylphosphinobenzaldehyde with the diamines 1,2-ethylenediamine, 1,3-propylenediamine, (*S,S*)-1,2-disopropyl-1,2-diaminoethane, and (*R,R*)-1,2-diphenyl-1,2-diaminoethane. Some complexes could also be obtained for the first time in a one-pot template synthesis under mild reaction conditions. Single crystal X-ray diffraction studies of the complexes revealed a *trans* distorted octahedral structure around the iron. The *i*Pr or Ph substituents on the diamine were found to be axial in the five-membered Fe−N−CHR−CHR−N− ring of the chiral P−N−N−P ligands. A steric clash between the imine hydrogen and the substituent probably determines this stereochemistry. The diaminodiphosphine complex has longer Fe−N and Fe−P bonds than the analogous diiminodiphosphine complex. The new iron compounds were used as precatalysts for the hydrogenation of acetophenone. The complexes without axial substituents on the diamine had moderate catalytic activity while that with axial Ph substituents had low activity but fair (61%) enantioselectivity for the asymmetric hydrogenation of acetophenone. The fact that the diaminodiphosphine complex has a slightly higher activity than the corresponding diiminodiphosphine complex suggests that hydrogenation of the imine groups in the P−N−N−P ligand may be important for catalyst activation. Evidence is provided, including the first density-functional theory calculations on iron-catalyzed outer-sphere ketone hydrogenation, that the mechanism is similar to that of ruthenium analogues.

Introduction

Replacing homogeneous catalysts based on platinum group metals with those based on first row transition metals is an attractive challenge. Iron-based catalysts would be desirable owing to their potentially lower cost, toxicity, and environmental impact.[1] Until recently the known homogeneous hydrogenation catalysts of iron had low activity relative to platinum metal catalysts,[2,3] apart from Chirik's iron catalysts for olefin and aryl azide hydrogenation[4−6] and the achiral iron catalyst recently reported by Casey et al. for ketone and imine hydrogenation.[7] There are also reports of iron-catalyzed hydrogenation of alkynes[8] and transfer hydrogenation of ketones and olefins[7−11] and enantioselective hydros-

* To whom correspondence should be addressed. E-mail: rmorris@chem.utoronto.ca. Phone: 1-416-978-6962. Fax: 1-416-978-6962.

(1) Enthaler, S.; Junge, K.; Beller, M. *Angew. Chem., Int. Ed.* **2008**, *47*, 3317–3321.
(2) Bolm, C.; Legros, J.; Le Paih, J.; Zani, L. *Chem. Rev.* **2004**, *104*, 6217–6254.
(3) Marko, L.; Palagyi, J. *Trans. Met. Chem.* **1983**, *8*, 207–209.
(4) Bart, S. C.; Lobkovsky, E.; Chirik, P. J. *J. Am. Chem. Soc.* **2004**, *126*, 13794–13807.
(5) Bart, S. C.; Hawrelak, E. J.; Lobkovsky, E.; Chirik, P. J. *Organometallics* **2005**, *24*, 5518–5527.
(6) Bart, S. C.; Lobkovsky, E.; Bill, E.; Chirik, P. J. *J. Am. Chem. Soc.* **2006**, *128*, 5302–5303.
(7) Casey, C. P.; Guan, H. *J. Am. Chem. Soc.* **2007**, *129*, 5816–5817.
(8) Bianchini, C.; Meli, A.; Peruzzini, M.; Frediani, P.; Bohanna, C.; Esteruelas, M. A.; Oro, L. A. *Organometallics* **1992**, *11*, 138–145.
(9) Bianchini, C.; Farnetti, E.; Graziani, M.; Peruzzini, M.; Polo, A. *Organometallics* **1993**, *12*, 3753–3761.

10.1021/ic801518h CCC: $40.75
Published on Web 11/26/2008

Chart 1

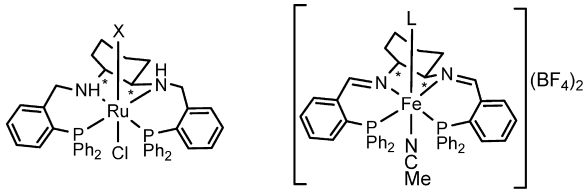

trans-RuXCl{(*R,R*)-cyP$_2$(NH)$_2$}
X = Cl, H

trans-[FeL(MeCN){(*R,R*)-cyP$_2$N$_2$}][BF$_4$]$_2$
L = MeCN, CO, NC*t*Bu

ilylation of ketones[12] under relatively mild conditions. Gao and co-workers reported that mixing [Et$_3$NH][Fe$_3$H(CO)$_{11}$] with chiral diaminodiphosphine P−NH−NH−P ligands produced moderately active and selective catalysts for the asymmetric transfer hydrogenation of ketones.[13]

Gao et al. showed previously that the ruthenium complex *trans*-RuCl$_2$\{(*R,R*)-cyP$_2$(NH)$_2$\} with the diaminodiphosphine ligand ((*R,R*)-{PPh$_2$(2-C$_6$H$_4$)CH$_2$NHC$_6$H$_{10}$NHCH$_2$(2-C$_6$H$_4$)PPh$_2$} (Chart 1) was a precatalyst for the active and selective asymmetric transfer hydrogenation of ketones using basic isopropanol as the source of the hydrogen.[14] The presence of the NH is important since the analogous complex *trans*-RuCl$_2$\{(*R,R*)-cyP$_2$N$_2$\} containing the diiminodiphosphine ligand was found to be much less active. Rautenstrauch's group and our group reported that related ruthenium complexes with the tetradentate P−NH−NH−P ligands ethP$_2$(NH)$_2$ ({PPh$_2$(2-C$_6$H$_4$)CH$_2$NH(CH$_2$)$_2$NHCH$_2$(2-C$_6$H$_4$)PPh$_2$}) and (*R,R*)-cyP$_2$(NH)$_2$ (Chart 1) are very active precatalysts for the H$_2$-hydrogenation of ketones.[15−17]

Motivated by these results, we were wondering whether similar well-defined iron complexes could be used as precatalysts for the hydrogenation of ketones. We recently reported that the complex *trans*-[Fe(NCMe)$_2$\{(*R,R*)-cyP$_2$N$_2$\}][BF$_4$]$_2$ (Chart 1) containing a diiminodiphosphine ligand ((*R,R*)-{PPh$_2$(2-C$_6$H$_4$)CH=NC$_6$H$_{10}$*N*=CH(2-C$_6$H$_4$)PPh$_2$} was active and somewhat enantioselective for H$_2$ hydrogenation of acetophenone to 1-phenylethanol with 27% e.e. while related complexes with carbonyl or isonitrile ligands (Chart 1) were very active and moderately selective for the asymmetric transfer hydrogenation of ketones.[18]

The present contribution reports the syntheses and characterization of related well-defined Fe complexes where the diamine precursor to the diiminodiphosphine ligand is varied to study the effect of the ligand structure on the activity and selectivity of iron-based asymmetric hydrogenation catalysts. Thus, the achiral tetradentate diiminodiphosphine ligands ethP$_2$N$_2$ ({PPh$_2$(2-C$_6$H$_4$)CH=N(CH$_2$)$_2$N=CH(2-C$_6$H$_4$)PPh$_2$}) and prP$_2$N$_2$ ({PPh$_2$(2-C$_6$H$_4$)CH=N(CH$_2$)$_3$N=CH(2-C$_6$H$_4$)-PPh$_2$}) are employed, as well as the diaminodiphosphine ligand ethP$_2$(NH)$_2$ ({PPh$_2$(2-C$_6$H$_4$)CH$_2$NHCH$_2$-}$_2$), to probe the need for the NH groups in ketone hydrogenation. Gao et al. reported the synthesis of the dicationic complexes [Fe(NCMe)$_2$(ethP$_2$N$_2$)][ClO$_4$]$_2$ and [Fe(NCMe)$_2$(ethP$_2$(NH)$_2$)]-[ClO$_4$]$_2$ but did not report the crystal structures or catalytic activity of these.[19] We also use for the first time the chiral tetradentate diiminodiphosphine ligands \{(*S,S*)-(*i*Pr-ethP$_2$N$_2$)\} ((*S,S*)-{PPh$_2$(2-C$_6$H$_4$)CH=NCH(*i*Pr)-}$_2$) and \{(*R,R*)-(ph-ethP$_2$N$_2$)\} ((*R,R*)-{PPh$_2$(2-C$_6$H$_4$)CH=NCH(Ph)-}$_2$[20] in the synthesis of iron complexes to probe the effect of substitutions at the diamine on the catalyst activity and enantioselectivity.

Results and Discussion

Synthesis and Characterization. The reaction of FeCl$_2$ or [Fe(H$_2$O)$_6$][BF$_4$]$_2$ with the neutral ligands ethP$_2$N$_2$, prP$_2$N$_2$, (*S,S*)-*i*Pr-ethP$_2$N$_2$, and (*R,R*)-Ph-ethP$_2$N$_2$ in acetonitrile gave the corresponding iron complexes [Fe(NCMe)$_2$(ethP$_2$N$_2$)]-[FeCl$_4$] (**1**), [Fe(NCMe)$_2$(ethP$_2$N$_2$)][BF$_4$]$_2$ (**2**), [Fe(NCMe)$_2$(prP$_2$N$_2$)][BF$_4$]$_2$ (**4**), [Fe(NCMe)$_2$\{(*S,S*)-(*i*Pr-ethP$_2$N$_2$)\}][BF$_4$]$_2$ (**5**), and [Fe(NCMe)$_2$\{(*R,R*)-(ph-ethP$_2$N$_2$)\}][BF$_4$]$_2$ (**6**) in good yields (Scheme 1, Method A and B). We also found that a new, in situ one-pot template synthesis of 2-(diphenylphosphino)benzaldehyde and ethylenediamine or 1,3-diaminopropane with [Fe(H$_2$O)$_6$][BF$_4$]$_2$ in the presence of Na$_2$SO$_4$ produces compounds **2** and **4** in 68% and 84% yield, respectively (Scheme 1, Method C). A different template synthesis of related iron complexes was reported recently.[21] Further reaction of **2** with the sodium salt NaB\{Ar^f\}$_4$ (Ar^f = 3,5-(CF$_3$)$_2$C$_6$H$_3$) produces the complex [Fe(ethP$_2$N$_2$)(NCMe)$_2$][B\{Ar^f\}$_4$]$_2$ (**3**).

Complexes **1**−**6** were isolated in 64−93% yields as red-orange solids that are air stable for a few hours (both in the solid-state and in solution). They dissolve in CH$_2$Cl$_2$, MeCN, and DMSO to give a red-orange solution, but they are poorly soluble in CHCl$_3$, 2-propanol and insoluble in diethyl ether, THF, and hydrocarbons. Their spectroscopic properties are similar to those of the perchlorate salts reported by Gao et al.,[19] displaying the characteristic singlet in the ^{31}P\{^{1}H\} NMR spectrum at about 51−54 ppm and a singlet for the imine resonance at about 8.9−9.4 ppm in the ^{1}H NMR spectrum. The structures of compounds **1**, **2**, **4**, **5**, and **6** in the solid state were also established by X-ray crystallography (Figure 1). Bond distances and angles are shown in Table 1. Compound **2** crystallizes with three independent molecules

(10) Enthaler, S.; Erre, G.; Tse, M. K.; Junge, K.; Beller, M. *Tetrahedron Lett.* **2006**, *47*, 8095–8099.
(11) Enthaler, S.; Hagemann, B.; Erre, G.; Junge, K.; Beller, M. *Chem. Asian J.* **2006**, *1*, 598–604.
(12) Shaikh, N. S.; Enthaler, S.; Junge, K.; Beller, M. *Angew. Chem., Int. Ed.* **2008**, *47*, 2497–2501.
(13) Chen, J. S.; Chen, L. L.; Xing, Y.; Chen, G.; Shen, W. Y.; Dong, Z. R.; Li, Y. Y.; Gao, J. X. *Acta Chim. Sin. (Huaxue Xuebao)* **2004**, *62*, 1745.
(14) Gao, J. X.; Ikariya, T.; Noyori, R. *Organometallics* **1996**, *15*, 1087–1089.
(15) Rautenstrauch, V.; Hoang-Cong, X.; Churlaud, R.; Abdur-Rashid, K.; Morris, R. H. *Chem.—Eur. J.* **2003**, *9*, 4954–4967.
(16) Li, T.; Churlaud, R.; Lough, A. J.; Abdur-Rashid, K.; Morris, R. H. *Organometallics* **2004**, *23*, 6239–6247.
(17) Clapham, S. E.; Hadzovic, A.; Morris, R. H. *Coord. Chem. Rev.* **2004**, *248*, 2201–2237.
(18) Sui-Seng, C.; Freutel, F.; Lough, A. J.; Morris, R. H. *Angew. Chem., Int. Ed. Engl.* **2008**, *47*, 940–943.
(19) Gao, J. X.; Wan, H. L.; Wong, W. K.; Tse, M. C.; Wong, W. T. *Polyhedron* **1996**, *15*, 1241–1251.
(20) Gao, J.-X.; Zhang, H.; Yi, X.-D.; Xu, P.-P.; Tang, C.-L.; Wan, H.-L.; Tsai, K.-R.; Ikariya, T. *Chirality* **2000**, *12*, 383–388.
(21) Mikhailine, A. A.; Kim, E.; Dingels, C.; Lough, A. J.; Morris, R. H. *Inorg. Chem.* **2008**, *47*, 6587–6589.

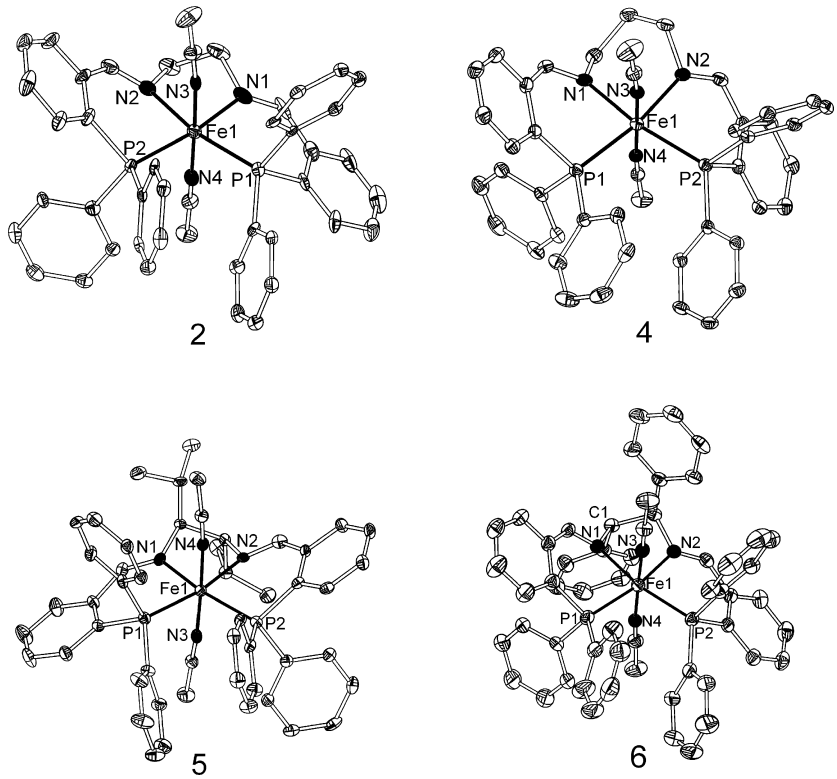

Figure 1. Structures of complexes **2**, **4**, **5**, and **6**. Thermal ellipsoids are shown at 30% probability. The counter-ions, hydrogen atoms and solvent molecules are omitted for clarity. Only one of the three independent molecules of compound **2** is shown.

Scheme 1. Preparation of the Fe(II) Complexes **1**−**6**

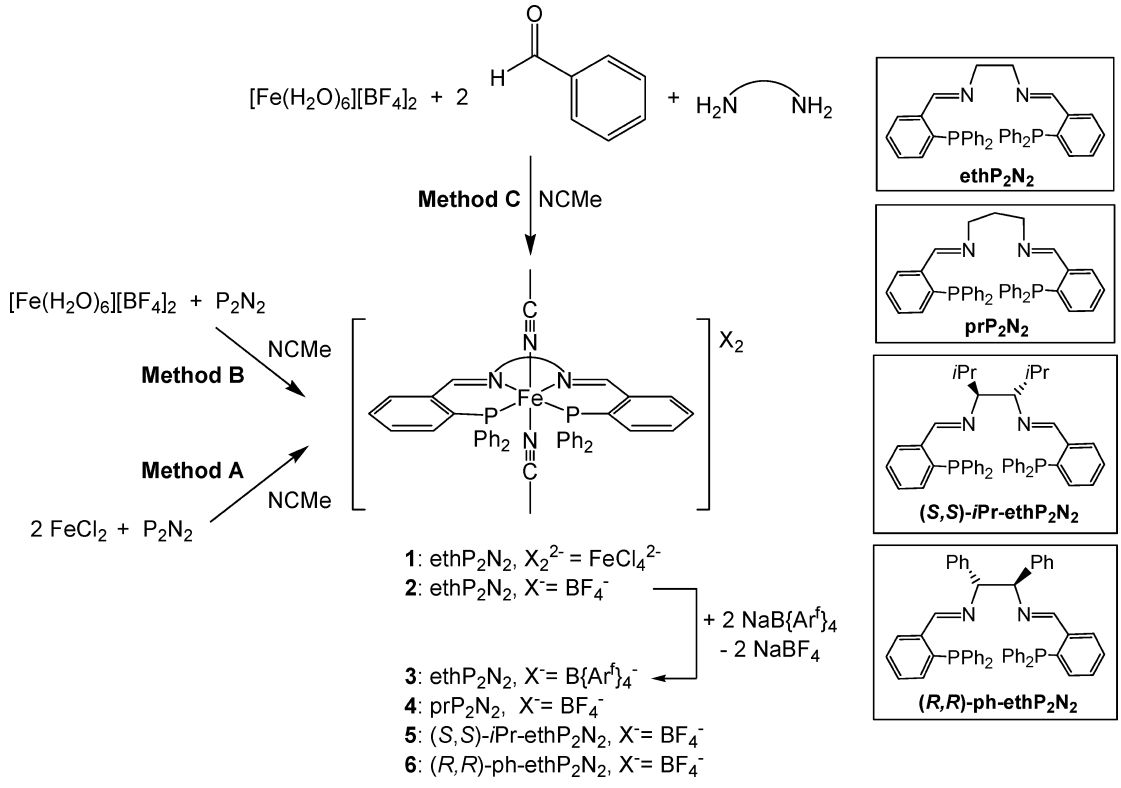

in the asymmetric unit, but all bond distances and angles are in a similar range, so only one molecule is discussed.

The complexes are distorted *trans* octahedral. The Fe−P distances are between those observed for the low-spin iron(II) complex *cis*-[Fe(CO)(NCMe)($PEt_2CH_2NMeCH_2PEt_2$)($PMe_2CH_2PMe_2$)][BF_4]$_2$ (Fe−P 2.30−2.38 Å)[22] and those observed in the complexes *trans*-[FeH(NCMe)($PEt_2CH_2NMeCH_2PEt_2$)($PMe_2CH_2PMe_2$)][BF_4] (Fe−P 2.20−2.22 Å)[22] and *trans*-[Fe(H_2)H(dppe)$_2$][BPh_4] (Fe−P 2.23−2.25 Å)[23] while the Fe−N(3) and Fe−N(4) distances to the MeCN ligands

Table 1. Selected Bond Distances (Å) and Angles (deg) for Complexes **1**, **2**, **4**, **5**, **6**, and **7a**

	1	2[a]	4	5	6	7a
Fe1−N1	2.013(4)	2.044(8)	2.026(3)	2.030(40	2.011(3)	2.068(4)
Fe1−N2	2.011(3)	1.986(2)	2.038(3)	2.018(4)	2.021(3)	2.087(3)
Fe1−N3	1.929(3)	1.903(9)	1.911(3)	1.916(4)	1.910(3)	1.916(4)
Fe1−N4	1.928(4)	1.933(9)	1.914(3)	1.920(4)	1.920(4)	1.890(4)
Fe1−P1	2.2879(13)	2.256(2)	2.280(1)	2.2825(14)	2.274(2)	2.3379(14)
Fe1−P2	2.2621(11)	2.279(3)	2.290(1)	2.2715(14)	2.268(2)	2.3221(15)
N4−Fe1−N3	174.88(15)	175.2(23)	179.39(13)	178.05(17)	178.56(15)	177.67(19)
N1−Fe1−N2	82.73(13)	82.6(3)	85.4(1)	80.90(16)	81.62(13)	82.56(15)
P2−Fe1−P1	98.83(4)	102.41(9)	105.35(4)	101.29(5)	102.84(5)	102.32(5)
N1−Fe1−P1	171.89(9)	87.6(2)	84.97(8)	90.03(12)	86.67(10)	88.36(11)

[a] Data for one of three molecules in the unit cell. Those for the other two are very similar.

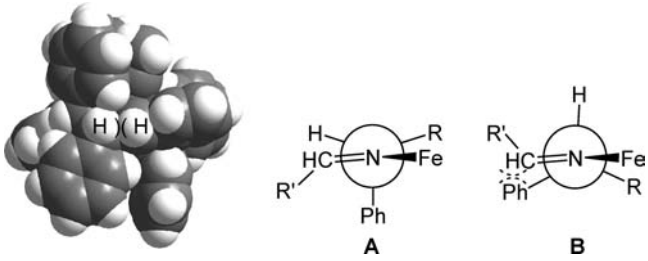

Figure 2. Space filling model of **6** and Newman Projections along the N1−C1 axis emphasizing the close contact of an equatorial ethylene hydrogen and an imine hydrogen (R = CHPh, R′ = C_6H_4) in conformation **A** and the steric clash of conformation **B**.

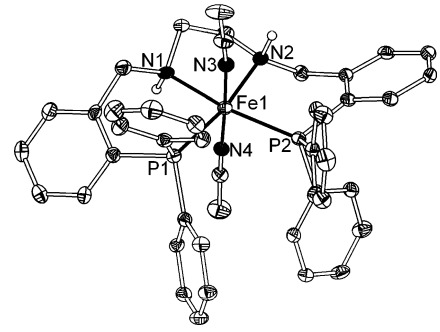

Figure 3. Structure of complex **7a**. Thermal ellipsoids are shown at 30% probability. The counter-ions, the hydrogen atoms (except NH), and the solvent molecules are omitted for clarity.

are similar to that of the first (the carbonyl) complex. The main distortions from octahedral angles are due to the geometric requirements of the P−N−N−P ligands where the N−Fe−N angles are small (80.9 to 82.7° for the complexes with 5-membered rings and 85.4(1)° for the 6-membered ring of **4**) and the P−Fe−P angles are large (98.8 to 105.4°). In complexes **5** and **6**, the (*S,S*)-substituted isopropyl and the (*R,R*)-substituted phenyl groups occupy the axial positions of the 5-membered Fe−N−CHR−CHR−N− ring. A reason for this might be the steric effect of the C*H*=N protons. The space filling model of **6** (Figure 2) shows that the imine protons are close but avoid the ethylene hydrogens (the favored conformation **A** in the Newman Projection of Figure 2) while they would clash with the phenyl rings on the ethylene backbone if these were in the equatorial position (disfavored conformation **B**). Of 204 crystal structures of complexes containing the diamine $NH_2CHPhCHPhNH_2$ as a bidentate ligand or its derivatives as bidentate or polydentate ligands reported in the Cambridge Crystallographic Database, we find that only 25 have axial phenyl substituents on the five-membered chelate rings. Of these, four are bidentate with bulky groups on nitrogen, one is tridentate, and the rest are tetradentate. In almost all of these tetradentate structures there is a steric basis for the axial orientation of the phenyls. The complex *trans*-$[Fe(MeCN)_2\{cyP_2N_2\}][BF_4]_2$ has a less sterically demanding cyclohexyl ring fused to the equatorial positions of the 5-membered ring.

The reaction of the tetradentate diaminodiphosphine ligand $ethP_2(NH)_2$ with $[Fe(H_2O)_6][BF_4]_2$ in acetonitrile produces the purple complex *trans*-$[Fe(NCMe)_2(ethP_2(NH)_2)][BF_4]_2$

Scheme 2. Preparation of Complex **7** As Two Isomers

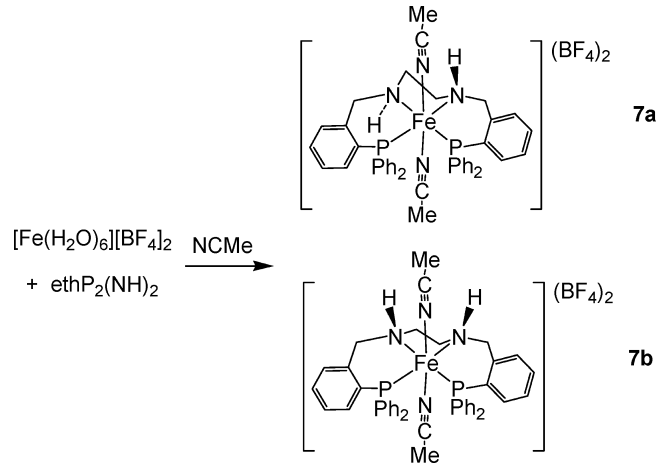

(**7**) (Scheme 2). The $^{31}P\{^1H\}$ NMR spectra shows two singlets at 38 and 46 ppm, and the ^1H NMR exhibits two sets of signals indicating that a mixture of two isomers in a ratio **7a**/**7b** 2.4:1.0 was obtained. The signals for the N−CH_2−CH_2−N protons in complex **7** appear as multiplets centered at 2.57 and 3.12 for **7a** and 2.95 and 3.0 ppm for **7b**. The H,H-COSY spectrum indicates that these signals form an AA′BB′ spin system. Unambiguous assignment of the amine protons was achieved by adding a few drops of D_2O to the NMR sample, which caused the two multiplets observed for N*H* at 4.42 for **7a** and 4.33 ppm for **7b** to disappear.

The structure of **7a** as determined by single crystal X-ray diffraction is shown in Figure 3. Bond distances and angles are given in Table 1. The Fe−P and Fe−N bond distances to the P−NH−NH−P ligand in **7a** are all longer than the corresponding ones in the P−N−N−P ligand in complexes

(22) Henry, R. M.; Shoemaker, R. K.; Newell, R. H.; Jacobsen, G. M.; DuBois, D. L.; Rakowski DuBois, M. *Organometallics* **2005**, *24*, 2481–2491.
(23) Ricci, J. S.; Koetzle, T. F.; Bautista, M. T.; Hofstede, T. M.; Morris, R. H.; Sawyer, J. F. *J. Am. Chem. Soc.* **1989**, *111*, 8823–8827.

Scheme 3. Catalytic Hydrogenation of Acetophenone

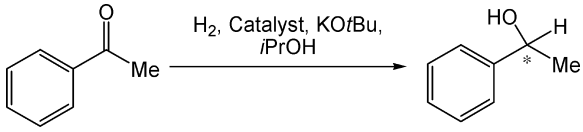

Table 2. Catalytic Hydrogenation of Acetophenone[a]

entry	C	S:C:B	*T* (°C)	PH_2 (atm)	time (h)	conv. (%)	e.e. (%)
1	**2**	225:1:15	50	15	18	5−15	
2	**2**	225:1:15	20	25	18	5	
3	**2**	225:1:15	50	25	18	70−95	
4	**3**	200:1:8	50	10	14	14	
5	**4**	225:1:15	50	25	18	80	
6	**5**	225:1:15	50	25	24	3	<5
7	**6**	225:1:15	50	25	18	4	61
8	**7**	225:1:15	20	25	18	4	
9	**7**	225:1:15	50	25	18	99	

[a] S = PhCOMe, C = catalyst, B = KO*t*Bu.

1, **2**, and **4**−**6** by 0.03−0.10 Å. Complex **7a** has an approximate C_2 axis in the FeP_2N_2 plane. The NH groups point to opposite sides of the plane of the P−NH−NH−P ligand, and the backbone is skewed through this plane. The other isomer, **7b**, likely has the two NH groups on the same side of the plane. These isomers readily interconvert in MeCN, possibly by NH deprotonation/reprotonation reactions as observed for related ruthenium complexes.[15,16]

Hydrogenation of Acetophenone. Complexes **2**−**7** were tested as catalyst precursors for the hydrogenation of acetophenone to 1-phenylethanol in basic isopropanol (Scheme 3) and the results are summarized in Table 2. Complex **2** provides a more active system at 25 atm H_2 than at 15 atm when the temperature is 50 °C (entries 3 vs 1 of Table 2). This pressure dependence is consistent with dihydrogen splitting being the turn-over limiting step as it is for the $RuHCl(cyP_2(NH)_2)$ catalyst system.[15] The use of the $B\{Ar^f\}_4^-$ anion (complex **3**) instead of the BF_4^- anion allowed some activity at 10 atm H_2 (entry 4) but the advantage was not sufficient to warrant further investigation, and a screening of different anions has not been done yet. Complex **2** provided a system that was even somewhat active at room temperature (entry 2). Thus the standard conditions for iron catalysis became 25 atm H_2 and 50 °C when the substrate to catalyst ratio is 225:1 and base/catalyst ratio is 15:1. Smaller ratios of base/catalyst provided poor reactivity; there is no hydrogenation if the base is omitted. Under the standard conditions complexes **2**, **4**, and **7** constitute moderately active precatalysts (Entries 3, 5, and 9) with activities comparable to that of *trans*-$[Fe(MeCN)_2\{cyP_2N_2\}]^{2+}$.[18] By contrast the chiral complexes **5** and **6** display poor reactivity with complex **5** providing essentially racemic 1-phenylethanol while **6** shows some enantioselectivity (61% e.e.) in favor of the S isomer. The bulky axial substituents of **6** and **7** as noted above must block access to the iron. In all cases the catalyst activity dies at the conversion noted in the Table 2.

The somewhat lower activity of **2** (entry 3) compared to **7** (entry 9) suggests that **2** might be converted to the same active hydride species as **7**, possibly *trans*-$FeH_2\{ethP_2(NH)_2\}$. In this regard we have demonstrated that diimine ligands on ruthenium undergo reduction to the

Scheme 4. Catalytic Cycle for the Outer Sphere Hydrogenation of Acetone Using $MH(NHCH_2CH_2NH_2)(PH_3)_2$ (M = Fe or Ru)

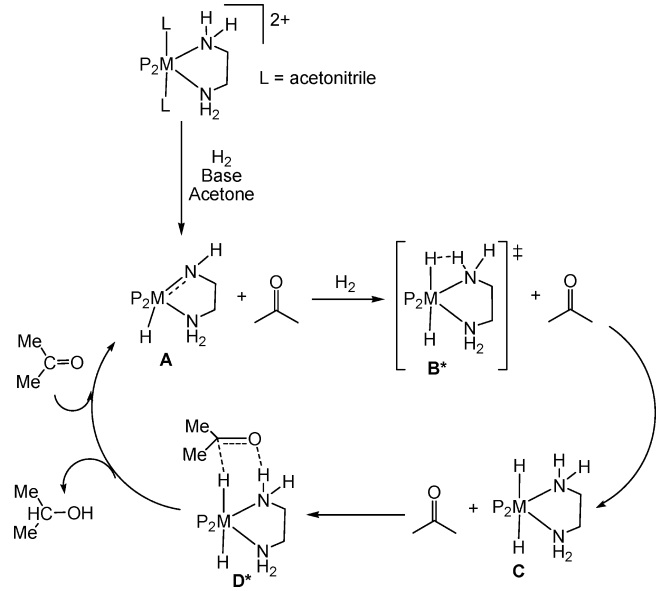

diamine before becoming active hydrogenation catalysts.[16] The complex *trans*-$FeH_2\{ethP_2(NH)_2\}$ would have the hydride and NH groups thought to be necessary for the efficient outer sphere transfer of hydride and proton to the ketone that is suspected for analogous ruthenium systems.[17] Both complexes **2** and **7** display low activity at room temperature (entries 2 and 8) with turnover frequencies (TOF) of about 1 h^{-1} but good reactivity at 50 °C (TOF at 99% conversion = 12 h^{-1} for **7**). The current systems have slightly lower activity than that of Casey's system (TOF 2 h^{-1} at 25 °C).[7]

Complexes **2**−**7** were also tested for the hydrogenation of acetophenone to 1-phenylethanol by transfer from basic isopropanol, but none of these complexes showed catalytic activity.

Density-Functional Theory (DFT) Calculations. Thus a possible mechanism for the asymmetric hydrogenation of acetophenone using catalysts **1**−**6** may involve dihydride species, the simplest of these being *trans*-$FeH_2\{ethP_2(NH)_2\}$. Owing to the large size of this dihydride, the tetradentate ligand has been simplified to one ethylene diamine and two PH_3 ligands for the present DFT study. Such a simplification was shown in a previous computational study on the analogous ruthenium system to have no significant effect on the core structures and relative energies of species.[24]

With the assumption that the mechanism of catalysis with iron is similar to that of ruthenium (with the catalytic cycle shown in Scheme 4) and that the iron species are low spin, we can calculate their structures and energetics and compare them to those of ruthenium.

The cycle begins with the hydrido-amido species **A** (Scheme 4, Figure 4) and acetone both of which have a relative free energy of 4.3 kcal/mol versus **A** and free isopropanol (Figure 5). For both iron and ruthenium, a very similar distorted trigonal bipyramidal geometry is predicted

(24) Li, T.; Bergner, I.; Haque, F. N.; Zimmer-De Iuliis, M.; Song, D.; Morris, R. H *Organometallics,* **2007**, *26*, 5940–5949.

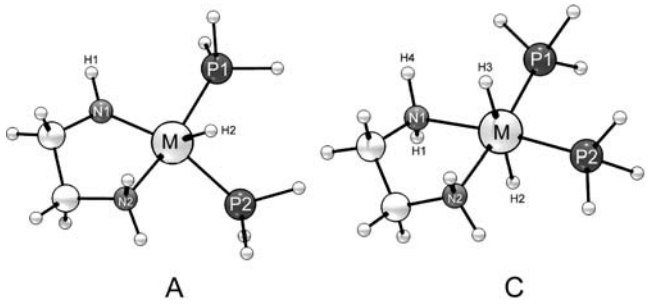

Figure 4. Calculated Structures of the hydrido-amido complex **A** and the *trans*-dihydride species **C**, where M = Fe or Ru. For bond distances and angles see the Supporting Information.

with the amido nitrogen N1, the hydride H2, and the phosphorus P2 occupying the equatorial positions. The M−N1 bond is short (1.84 Å for Fe, 1.94 Å for Ru), which reflects multiple bond character consistent with a dative p(N)→d(M) amido-metal π-bond. The negative charge (−0.6) on the amide nitrogen is similar for both species. The next step in the cycle is the heterolytic splitting of dihydrogen across the M−N1 bond via transition state **B*** (Figure 6).

The activation barrier for this step is 20.8 kcal/mol for iron and 20.9 kcal/mol for ruthenium. In the transition state structure **B***, the H3−H4 distance is elongated from 0.78 Å in free dihydrogen to nearly 1 Å for both iron and ruthenium. The APT (atomic polar tensor) charges indicate that the H−H bond is highly polarized (H3 −0.2, H4 +0.4) in each case. An analysis of the vibrational mode of the transition state with frequency 1056*i* cm^{-1} for iron and 1172*i* cm^{-1} for ruthenium reveals that the H3−H4 bond elongates and at the same time the geometry of N1 changes from trigonal planar to tetrahedral.

The cycle then proceeds to the *trans*-dihydride **C**, which, along with 1 equiv of acetone, has a relative free energy of 5.3 kcal/mol for iron and 2.3 kcal/mol for ruthenium. The dihydride **C** is the H_2 transfer agent in this cycle as H3 and H4 are oriented such that a oxygen of a ketone carbonyl group will interact with the proton on N1 of the diamine while, at the same time, the carbon of the ketone can orient close to the hydride on the metal. Such a transition state, **D***, was in fact located, and it has a relative free energy of 15.5 kcal/mol for iron and 4.3 kcal/mol for ruthenium. The H4−O1 and H3−C1 bond distances decrease while at the same time the geometry of C1 changes from trigonal planar to tetrahedral in the transition state vibrational mode with an imaginary frequency of 161.6*i* for Fe (c.f. 186.6*i* for Ru). The hydride on ruthenium has a greater negative charge than on iron, and the C−O bond is more polarized in the transition state with ruthenium than iron. Thus, electrostatics play a large part in lowering the barrier for ruthenium compared to iron. Overall, using either iron or ruthenium, the hydrogenation of acetone via the proposed mechanism is thermodynamically favorable by 4.3 kcal/mol.

Therefore, the calculations indicate that the splitting of dihydrogen is the turn-over limiting step in this mechanism for iron as it is for ruthenium, and the energetics are very similar. On the other hand, the H^+/H^- transfer to the ketone is a higher activation process for iron than ruthenium.

Conclusion

In summary, we have prepared and characterized some achiral and chiral iron complexes containing P−N−N−P and P−NH−NH−P ligands in the coordination sphere. These complexes are easily accessible by reaction of the neutral ligands with the Fe^{2+} salts $[Fe(H_2O)_6][BF_4]_2$ or $FeCl_2$. Thus, the compounds $[Fe(NCMe)_2(ethP_2N_2)][FeCl_4]$ (**1**), $[Fe(NCMe)_2(ethP_2N_2)][BF_4]$ (**2**), $[Fe(NCMe)_2(prP_2N_2)][BF_4]_2$ (**4**), $Fe(NCMe)_2\{(S,S)\text{-}(i\text{Pr-}ethP_2N_2)\}][BF_4]_2$, (**5**), $[Fe(NCMe)_2\{(R,R)\text{-}(ph\text{-}ethP_2N_2)\}][BF_4]_2$ (**6**), and $[Fe(NCMe)_2(ethP_2(NH)_2)][BF_4]_2$ (**7**) were obtained. We also have shown that **2** and **4** can be prepared in a one-pot template synthesis of 2-(diphenylphosphino)benzaldehyde and ethylenediamine or 1,3-diaminopropane with the iron precursor $[Fe(H_2O)_6][BF_4]_2$. We show for the first time that the diaminodiphosphine complex **7** has longer Fe−N and Fe−P bonds than the analogous diiminodiphosphine complex **2**.

Complexes **2**, **4**, and **7** have good activity for catalyzing the hydrogenation of acetophenone under the conditions reported for the related complex *trans*-$[Fe(NCMe)_2\{cyP_2N_2\}]]^{2+}$. All of these complexes have hydrogen atoms in axial positions of the diamine-derived backbone. Complexes **5** and **6** with axial *i*Pr and Ph groups, respectively, on the Fe−N−CHR−CHR−N− rings are much less active, presumably because access to the iron is blocked. In all cases the catalyst systems dies after 222 turnovers for **7**, 214 for **2**, 180 for **4**, 7 for **5**, and 9 for **6**.

The fact that the rate of hydrogenation increases with the pressure of dihydrogen and the fact that NH groups in the ligand appear to favor catalysis (with complex **7** slightly more active than **2**) point to similarities with the mechanism of action of related ruthenium catalysts. That is, the heterolytic splitting of dihydrogen may produce an H−Fe−N−H motif that permits the efficient outer sphere transfer of a hydride and a proton to the polar carbonyl group. The first DFT calculations indicate that this is a viable mechanism for iron.

Considering the fact that almost nothing is known about the iron-catalyzed hydrogenation of ketones, we plan to test a number of different ligand systems to get a better understanding of the influence of the ligand for this reaction. Mechanistic and kinetic studies are also in progress.

Experimental Section

General Procedures. All preparations and manipulations were carried out under an argon or nitrogen atmosphere using standard Schlenk and glovebox techniques. Dry, oxygen-free solvents were prepared by distillation from appropriate drying agents and employed throughout. The ethylenediamine and the 1,3-diaminopropane were distilled before use. All other commercially available reagents were used without further purification. The synthesis of $Na[B\{3,5\text{-}(CF_3)_2C_6H_3\}_4]$ ($NaB\{Ar^f\}_4$)[25,26] and the ligands $ethP_2N_2$, $ethP_2(NH)_2$ prP_2N_2, and (*R,R*)-ph-$ethP_2N_2$ have been reported previously.[20,27] The (*S,S*)-1,2-bis-isopropyl-1,2-diaminoethane di-

(25) Reger, D. L.; Wright, T. D.; Little, C. A.; Lamba, J. J. S.; Smith, M. D. *Inorg. Chem.* **2001**, *40*, 3810–3814.
(26) Brookhart, M.; Grant, B.; Volpe, A. F., Jr. *Organometallics* **1992**, *11*, 3920–3922.
(27) Jeffery, J. C.; Rauchfuss, T. B.; Tucker, P. A. *Inorg. Chem.* **1980**, *19*, 3306–3315.

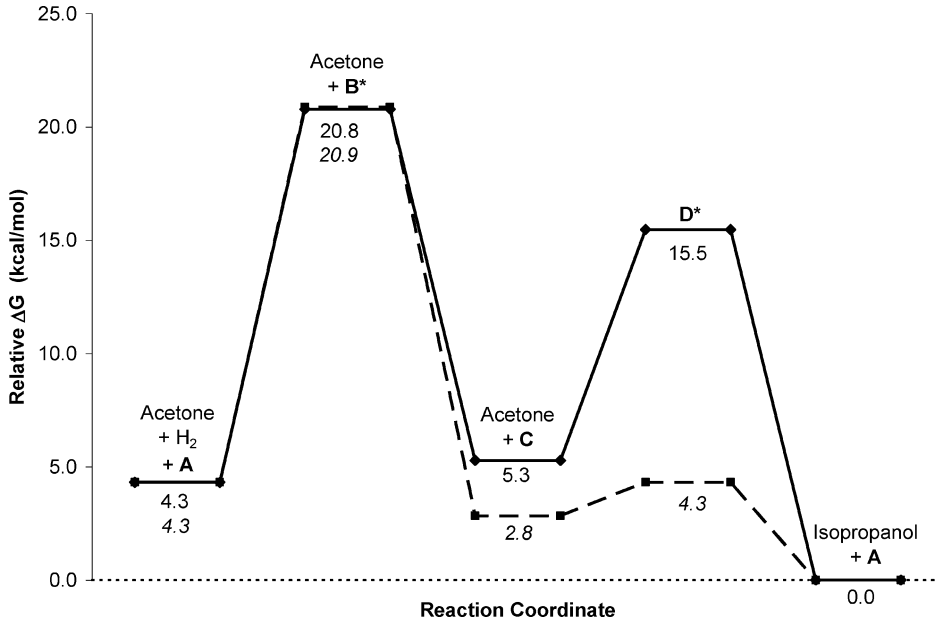

Figure 5. Reaction coordinate diagram (free energies at 298 K, 1 atm) for the hydrogenation of acetone starting with **A**, acetone, and dihydrogen. The solid line is the cycle with iron as the metal center, while the dotted line represents the cycle with ruthenium. The free energies reported are relative to the sum of the free energies of **A** and isopropanol.

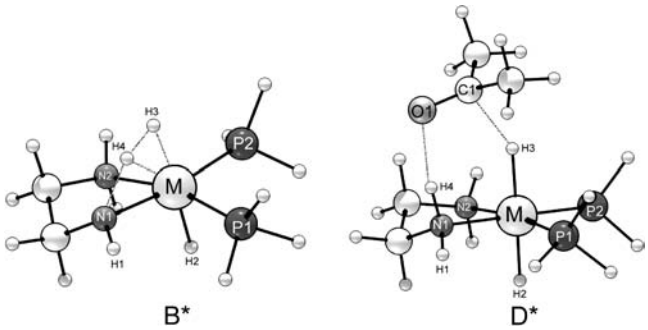

Figure 6. Calculated transition state structures of dihydrogen splitting, **B***, and the concerted transfer of dihydrogen to acetone, **D***. For the bond distances and angles see the Supporting Information.

hydrochloride was provided by DiaminoPharm Inc. The mass spectroscopy and elemental analyses were performed at the University of Toronto, and all samples were handled under argon for the EA. Varian Gemini 400 and 300 MHz spectrometers were employed for recording ^{1}H (400 and 300 MHz), ^{13}C{^{1}H} (100 and 75 MHz), and ^{31}P{^{1}H} (121 MHz) NMR spectra at ambient temperature. The ^{1}H and ^{13}C NMR spectra were referenced to solvent resonances, as follows: 7.26 and 77.16 ppm for C*H*Cl$_3$ and *C*DCl$_3$, 1.94 and 1.24 ppm for C*H*$_3$CN and *C*D$_3$CN). The ^{31}P NMR spectra were referenced to 85% H$_3$*P*O$_4$ (0 ppm). Gas chromatography was carried out on a Perkin-Elmer Autosystem XL. All infrared spectra were recorded on a Nicolet 550 Magna-IR spectrometer.

Synthesis of (*S*,*S*)-{PPh$_2$(2-C$_6$H$_4$)CH=NCH(*i*Pr)-}$_2$. A solution of (*S*,*S*)-1,2-bis-isopropyl-1,2-diaminoethane dihydrochloride (220 mg, 1.01 mmol), 2-(diphenylphosphino)benzaldehyde (579 mg, 1.99 mmol), triethylamine (406 μL, 3.03 mmol), and anhydrous Na$_2$SO$_4$ (834 mg, 5.87 mmol) in CHCl$_3$ was refluxed for 24 h. An orange suspension was obtained and evaporated to dryness. THF (10 mL) was added, and the mixture was filtered. The resulting filtrate was concentrated to about 1 mL and was layered with 15 mL of EtOH. A beige powder precipitated and was isolated by filtration (619 mg, 90%). ^{1}H NMR (300 MHz; CDCl$_3$): 8.71 (d, *J* 4.8, C*H*=N), 8.02−7.98, 7.35−7.16, 6.91−6.78, (m, Ar*H*), 2.99−2.96 (m, N−C*H*), 1.78−1.67 (m, C*H*-CH$_3$), 0.54−0.49 (m, C*H*$_3$).^{13}C{^{1}H} NMR (100 MHz, CDCl$_3$): 159.3 (d, *J* 21, H*C*=N), 140.1 (d, *J* 19, *Ar*), 136.9−136.7 (m, *Ar*), 134.1−133.8 (m, *Ar*), 133.1 (s, *Ar*), 129.7 (s, *Ar*), 128.7−128.4 (m, *Ar*), 78.12 (s, *C*H-*i*Pr), 28.45 (s, *C*H), 19.7, 18.4 (s, *C*H$_3$). ^{31}P{^{1}H} NMR (121 MHz; CDCl$_3$): −13.22 (s). Anal. Calcd for C$_{46}$H$_{46}$N$_2$P$_2$: C, 80.2; H, 6.73; N, 4.07%. Found: C, 79.26; H, 6.84; N, 4.96%. HRMS-EI (*m*/*z*): [M]$^+$ calcd for C$_{46}$H$_{46}$N$_2$P$_2$ 688.8184, found 688.3248. Selected IR (KBr) 1634 cm^{-1} (ν $_{C=N}$).

Synthesis of *trans*-[Fe(NCMe)$_2$(ethP$_2$N$_2$)][FeCl$_4$], (1). Method A. FeCl$_2$ (80 mg, 0.6 mmol) was added to a stirred MeCN suspension (10 mL) of ethP$_2$N$_2$ (200 mg, 0.3 mmol) at ambient temperature. The resulting orange-red mixture was stirred for 30 min. The product precipitated as an orange powder and was isolated by filtration (220 mg, 78%). Recrystallization from a CD$_3$CN solution in a NMR tube yielded red crystals suitable for X-ray diffraction studies and elemental analysis. ^{1}H NMR (300 MHz; CD$_3$CN): 8.99 (br, C*H*=N), 7.76−6.63 (m, Ar*H*), 6.03 (br, Ar*H*), 4.31, 2.87 (br, C*H*$_2$), 2.30 (s, C*H*$_3$CN). ^{31}P{^{1}H} NMR (161 MHz; CD$_3$CN): 54.05 (s). Anal. Calcd for C$_{44}$H$_{40}$N$_4$P$_2$Cl$_4$Fe$_2$: C, 56.2; H, 4.29; N, 5.96%. Found: C, 56.23; H, 4.45; N, 5.88%.

Synthesis of *trans*-[Fe(NCMe)$_2$(ethP$_2$N$_2$)][BF$_4$], (2). Method B. A suspension of ethP$_2$N$_2$ (149 mg, 0.25 mmol) in 5 mL of MeCN was added to a solution of [Fe(H$_2$O)$_6$][BF$_4$]$_2$ (84 mg, 0.25 mmol) in MeCN (10 mL). After stirring for 1 h, the red solution was concentrated to 1 mL, and 10 mL of Et$_2$O was added. A purple powder precipitated. The powder was isolated and washed with hexane. (200 mg, 87%). Crystals suitable for X-ray diffraction studies were obtained from a MeCN/Et$_2$O solution. ^{1}H NMR (400 MHz, CDCl$_3$): 9.46 (s, C*H*=N), 8.07−6.71 (m, Ar*H*), 4.35 (s, C*H*$_2$), 2.00 (s, C*H*$_3$CN); ^{31}P{^{1}H} NMR (161 MHz, CDCl$_3$) 54.4 (s). Anal. Calcd for C$_{44}$H$_{40}$N$_4$B$_2$F$_8$P$_2$Fe: C, 57.68; H, 4.40; N, 6.12%. Found: C, 57.16; H, 4.40; N, 5.86%.

Method C. A solution of [Fe(H$_2$O)$_6$][BF$_4$]$_2$ (100 mg, 0.29 mmol), 2-(diphenylphosphino)benzaldehyde (172 mg, 0.59 mmol), and 1,2-diaminoethane (20 μL, 0.29 mmol) in 5 mL of MeCN was refluxed for 1 h. The resulting red solution was concentrated to about 1 mL, and 10 mL of Et$_2$O were added. A red powder precipitated

Table 3. Summary of Crystal Data, Details of Intensity Collection, and Least-Squares Refinement Parameters for Complexes **1, 2**, **4**, **5**, **6**, and **7a**[a]

	1	2	4	5	6	7a
formula	$C_{44}H_{40}B_2F_8N_4P_2Fe_2Cl_4$. 3MeCN	$C_{44}H_{40}B_2F_8N_4P_2Fe$	$C_{45}H_{36}B_2F_8N_4P_2Fe$	$C_{50}H_{52}B_2F_8N_4P_2$ Fe. MeCN	$C_{56}H_{48}B_2F_8FeN_4N_2$	$C_{44}H_{44}B_2F_8FeN_4P_2$. MeCN
Fw	1063.40	916.21	924.19	1041.42	1068.39	961.30
size, mm	0.16 × 0.16 × 0.16	0.14 × 0.16 × 0.20	0.17 × 0.26 × 0.32	0.13 × 0.16 × 0.20	0.22 × 0.22 × 0.16	0.04 × 0.12 × 0.15
lattice type	tetragonal	orthorhombic	monoclinic	orthorhombic	monoclinic	monoclinic
space group	$I4_1/a$	$P2_12_12_1$	$P2_1/c$	$C222_1$	$C2$	$P2_1$
T, K	373	150	150	150	210	150
a, Å	33.049(5)	9.8340(3)	20.1739(10)	13.8857(4)	22.3773(5)	12.5831(6)
b, Å	33.049(5)	32.8133(10)	10.5412(2)	17.2819(5)	11.3226(4)	13.6522(10)
c, Å	19.333(4)	38.8071(14)	20.7331(10)	43.4423(9)	20.5795(7)	13.7334(8)
α, deg	90	90	90	90	90	90
β, deg	90	90	101.0440(15)	90	92.895(2)	107.936(3)
γ, deg	90	90	90	90	90	90
V, Å^3	21116(6)	12522.5(7)	4327.4(3)	10424.9(5)	5207.6(3)	2244.6(2)
Z	16	12	4	8	4	2
ρ_{calc}/Mg m^{-3}	1.338	1.458	1.419	1.327	1.363	1.422
μ(Mo Kα), mm^{-1}	0.853	0.512	0.495	0.419	0.422	0.480
F(000)	8768	5640	1888	4320	2200	992
range θ collected, deg	2.7 to 27.5	2.6 to 25.0	2.6 to 25.0	2.6 to 27.5	2.62 to 27.5	2.6 to 27.5
reflns collected/unique	67418/12075	50075/20664	23795/7163	23299/11696	22054/10781	14391/8383
R_1 ($I > 2\sigma(I)$)	0.0647	0.0807	0.0491	0.0656	0.057	0.0552
wR_2 (all data)	0.1242	0.1686	0.1131	0.1255	0.1597	0.0973
goodness of fit	1.049	1.005	0.996	0.944	1.027	0.985
parameters refined	591	1648	559	636	659	577
maximum peak in final ΔF map/e Å^{-3}	0.738	1.534	0.555	0.540	0.393	0.368

[a] Definition of R indices: $R_1 = \sum||F_o| - |F_c||/\sum|F_o|$; $wR_2 = [\sum[w(F_o^2 - F_c^2)^2]/\sum[w(F_o^2)^2]]^{1/2}$.

and was isolated by filtration and washed with hexane to give the analytically pure product (168 mg, 68%).

Synthesis of *trans*-[Fe(NCMe)$_2$(ethP$_2$N$_2$)][B{Ar^f}$_4$]$_2$ (3). NaB{Ar^f}$_4$ (85 mg, 0.096 mmol) was added to a CH_2Cl_2 solution (4 mL) of [Fe(MeCN)$_2$(ethP$_2$N$_2$)][BF$_4$]$_2$ (44 mg, 0.048 mmol). After stirring for 30 min, the resulting orange mixture was filtered through a small pad of Celite and evaporated to dryness to give an orange powder (110 mg, 93%). ^{1}H NMR (400 MHz, $CDCl_3$): 8.90 (s, C*H*=N), 7.70−6.57 (m, Ar*H*), 3.75 (s, CH_2), 2.00 (s, CH_3CN). ^{31}P{^{1}H} NMR (161 MHz, $CDCl_3$): 51.5 (s). Anal. Calcd for $C_{108}H_{64}N_4B_2F_{48}P_2Fe_1$: C, 52.54; H, 2.61; N, 2.27. Found: C, 52.95; H, 2.31; N, 2.0.

Synthesis of *trans*-[Fe(NCMe)$_2$(prP$_2$N$_2$)][BF$_4$]$_2$, (4). Method B. A solution of prP$_2$N$_2$ (408 mg, 0.66 mmol) in 15 mL of MeCN was added dropwise to a solution of [Fe(H$_2$O)$_6$][BF$_4$]$_2$ (220 mg, 0.65 mmol) in MeCN (10 mL). After stirring for 3 h, the resulting red solution was concentrated to about 1 mL, and 30 mL of hexane were added. A red-orange powder precipitated and was isolated by filtration and washed with hexane (530 mg, 87%). ^{1}H NMR (300 MHz, CD_3CN): 8.99 (s, C*H*=N), 7.82−6.51 (m, Ar*H*), 3.62 (br, N−CH_2), 2.28 (br, CH_2−CH_2−CH_2), 1.94 (s, CH_3CN). ^{31}P{^{1}H} NMR (121 MHz, CD_3CN): 51.3 (s). Anal. Calcd for $C_{45}H_{40}N_4B_2F_8P_2Fe_1$: C, 58.23; H, 4.34; N, 6.04. Found: C, 57.73; H, 3.82; N, 5.72.

Method C. A solution of [Fe(H$_2$O)$_6$][BF$_4$]$_2$ (100 mg, 0.29 mmol), 2-(diphenylphosphino)benzaldehyde (172 mg, 0.59 mmol), and 1,3-diaminopropane (25 μL, 0.29 mmol) in 5 mL of MeCN was stirred at ambient temperature for 1 h. The resulting red solution was concentrated to about 1 mL, and 10 mL of Et$_2$O were added. A red-orange powder precipitated and was isolated by filtration and washed with hexane (210 mg, 84%).

Synthesis of *trans*-[Fe(NCMe)$_2${(*S*,*S*)-(iPr-ethP$_2$N$_2$)}][BF$_4$]$_2$ (5). A solution of (*S*,*S*)-(eth-*i*PrP$_2$N$_2$) (239 mg, 0.35 mmol) and [Fe(OH$_2$)$_6$][BF$_4$]$_2$ (117 mg, 0.35 mmol) in MeCN (10 mL) was stirred for 20 min at ambient temperature.. The resulting red solution was concentrated to 1 mL, and 10 mL of Et$_2$O were added. A red-orange powder precipitated and was isolated by filtration and washed with Et$_2$O (259 mg, 75%). Vapor diffusion of diethyl ether into a solution of [Fe(NCMe)$_2${(*S*,*S*)-(*i*Pr-ethP$_2$N$_2$)}][BF$_4$]$_2$ in acetonitrile yielded red crystals suitable for X-ray diffraction studies and elemental analysis. ^{1}H NMR (300 MHz, $CDCl_3$): 9.39 (s, C*H*=N), 8.22−8.20, 7.79−6.73 (m, Ar*H*), 3.91 (d, *J* 9, N−C *H*), 2.00 (br, C*H*), 1.73 (s, CH_3CN), 1.18 (d, *J* 6, CH_3), 0.46 (d, *J* 6, CH_3). ^{31}P{^{1}H} NMR (121 MHz, $CDCl_3$): 52.3 (s). Anal. Calcd for $C_{50}H_{52}N_4B_2F_8P_2Fe_1 \cdot 1.25\ CHCl_3$: C, 53.55; H, 4.67; N, 4.87. Found: C, 53.56; H, 4.69; N, 5.09.

Synthesis of *trans*-[Fe(NCMe)$_2${(*R*,*R*)-(ph-ethP$_2$N$_2$)}][BF$_4$]$_2$ (6). A solution of (*R*,*R*)-(ph-ethP$_2$N$_2$) (510 mg, 0.78 mmol) and [Fe(H$_2$O)$_6$][BF$_4$]$_2$ (260 mg, 0.78 mmol) in MeCN (10 mL) was stirred for 1 h at ambient temperature. The solution was evaporated, and the remaining red residue was washed with pentane. The analytically pure product was obtained after crystallization from MeCN/Et$_2$O as dark red crystals (510 mg, 64%). Recrystallization from a MeCN/MeOH/Et$_2$O solution yielded crystals suitable for X-ray diffraction studies. ^{1}H NMR (400 MHz, CD_3CN): 9.32 (s, C*H*=N), 7.82−7.21 (m, Ar*H*), 6.94 (m, Ar*H*), 6.85 (m, Ar *H*), 5.97 (s, N−C *H*), 1.96 (s, CH_3CN). ^{31}P{^{1}H} NMR (161 MHz, $CDCl_3$): 51.8 (s). Anal. Calcd for $C_{56}H_{48}N_4B_2F_8P_2Fe_1$: C, 62.95; H, 4.53; N, 5.24. Found: C, 62.69; H, 4.79; N, 5.81.

Synthesis of *trans*-[Fe(MeCN)$_2$(ethP$_2$(NH)$_2$)][BF$_4$]$_2$ (7). A suspension of ethP$_2$(NH)$_2$ (300 mg, 0.49 mmol) in 5 mL of MeCN was added to a solution of [Fe(H$_2$O)$_6$][BF$_4$]$_2$ (168 mg, 0.49 mmol) in MeCN (10 mL). After stirring for 1 h, the resulting purple solution was concentrated to 1 mL, and 10 mL of Et$_2$O were added. A purple powder precipitated and was isolated by filtration (405 mg, 91%). Recrystallization of a small portion of this solid by vapor diffusion of Et$_2$O into a MeCN solution of [Fe(NCMe)$_2$(ethP$_2$(NH)$_2$)][BF$_4$]$_2$ under N$_2$ yielded crystals of **7a** suitable for X-ray diffraction studies and elemental analysis. ^{1}H NMR (400 MHz, CD_3CN): **7a**+**7b** (ratio 2.4:1)**:** 7.68−6.31 (m, Ar*H*); **7a**: 4.42 (br, N*H*), 3.95 (br, CH_2), 3.12 (AA′, NCH_2CH_2N), 2.57 (BB′, NCH_2CH_2N), 1.96 (s, CH_3CN); **7b** 4.37 (d, *J* 14, CH_2), 4.33 (br t, *J* 10, N*H*), 4.05 (dd, *J* 14, *J* 10, CH_2), 3.00, 2.95 (AA′BB′, NCH_2CH_2N), 1.96 (s, CH_3CN); ^{31}P{^{1}H} NMR (121 MHz, CD_3CN): 46.1 (s, **7b**), 38.5 ppm (s, **7a**). Anal. Calcd For $C_{44}H_{44}N_4B_2F_8P_2Fe$: C, 57.43; H, 4.82; N, 6.09%. Found: C, 57.0; H, 4.73; N, 6.38%.

General Procedure for the Iron Catalyzed Asymmetric H_2-Hydrogenation of Acetophenone. In an Ar or N_2 glovebox, the iron complex (0.008 mmol) was suspended in 2 mL of 2-propanol and acetophenone (225 equiv) in 1 mL of 2-propanol. The solution of base was prepared by dissolution of KO*t*Bu (15 equiv) in 2 mL of 2-propanol. The substrate solution, then the base solution, and finally the suspension of precatalyst were injected into a 50 cm^3 Parr hydrogenator reactor at the desired pressure and temperature, maintained by use of a Fischer Scientific Isotemp 1016D water bath. The conversion and enantiomeric excess of the products were determined by GC using a Perkin-Elmer Autosystem XL apparatus with a chiral column (CP Chirasil-Dex CB 25 m × 2.5 mm), and utilizing an H_2 carrier gas at a column pressure of 6 psi, an injector temperature of 250 °C, and a FID of 275 °C. The retention times were acetophenone 5.0 min, (*R*)-1-phenylethanol 8.5 min, (*S*)-1-phenylethanol 9.1 min.

X-ray Crystal Structure Determinations. X-ray crystallographic data for **1**−**2** and **4**−**7** were collected on a Bruker−Nonius Kappa-CCD diffractometer using monochromated Mo Kα radiation and were measured using a combination of ϕ scans and ω scans with κ offsets, to fill the Ewald sphere. The data were processed using the Denzo-SMN package. Absorption corrections were carried out using SORTAV. The structure was solved and refined using SHELXTL V6.1 for full-matrix least-squares refinement that was based on F^2. All H atoms were included in calculated positions and allowed to refine in riding-motion approximation with U_{iso} tied to the carrier atom. Crystallographic data for the compounds is given in Table 3.

Computational Details. All calculations were performed using Gaussian03.[28] The calculations were performed on a workstation with two 2.8 GHz Opteron X2 with 4 GB of RAM and Red Hat Linux Enterprise Edition. All calculations used the rMPW1PW91[29] density functional method. Ruthenium and iron were treated with the SDD basis set to include relativistic effects and an effective core potential, and H, C, N, P, and O were treated with the triple-ζ basis set 6−311++G** which includes diffuse functionals and additional p-orbitals on H, as well as additional d-orbitals on C, N, P, and O. The structures were optimized in the gas phase at 1 atm of pressure and 298 K. Full vibrational analyses were performed on the optimized structure to obtain values of ΔG, ΔH, and ΔS. The QST2 or QST3 method was utilized to locate transition states. All transition states were found to have one imaginary frequency. The calculated APT charges are used.[30] The APT charge is the derivative of the forces on the atoms with respect to an applied external electric field and yields atomic charges that more accurately reflect the charge distribution rather than individual atomic charges.

Acknowledgment. NSERC Canada is thanked for a Discovery Grant to R.H.M., the Petroleum Research Fund, as administered by the American Chemical Society for a Type AC grant to R.H.M., le Fonds de Recherche sur la Nature et les Technologies Québec for a fellowship to C.S.S., and the Deutscher Akademischer Austauschdienst for a scholarships to A.M.P. and V.R. We thank Hyunwoo Kim and Prof. Jik Chin for a gift of (*S*,*S*)-1,2-bis-isopropyl-1,2-diaminoethane dihydrochloride.

Supporting Information Available: Details of the DFT calculations, a complete citation for reference 28, and crystallographic data for **1**, **2**, **4**, **5**, **6**, **7a** (cif). This material is available free of charge via the Internet at http://pubs.acs.org.

IC801518H

(28) Frisch, M. J. et al. *Gaussian03*, Rev. B.03; Gaussian, Inc.: Pittsburgh, PA, 2001.

(29) Adamo, C.; Barone, V. *J. Chem. Phys.* **1998**, *108*, 664–675.

(30) Cioslowski, J. *J. Am. Chem. Soc.* **1989**, *111*, 8333–8336.